

PTR: A Pre-trained Language Model for Trajectory Recovery

Tonglong Wei*
School of Computer and Information
Technology, Beijing Jiaotong
University
Beijing, China
{weitonglong}@bjtu.edu.cn

Yan Lin*
Youfang Lin
School of Computer and Information
Technology, Beijing Jiaotong
University
Beijing, China
{ylincs,yflin}@bjtu.edu.cn

Shengnan Guo†
School of Computer and Information
Technology, Beijing Jiaotong
University
Beijing, China
guoshn@bjtu.edu.cn

Jilin Hu
School of Data Science and
Engineering, East China Normal
University
Shanghai, China
jlhu@dase.ecnu.edu.cn

Gao Cong
Nanyang Technological University
Singapore
gaocong@ntu.edu.sg

Huaiyu Wan
School of Computer and Information
Technology, Beijing Jiaotong
University
Beijing, China
hywan@bjtu.edu.cn

Abstract

Spatiotemporal trajectory data is vital for web-of-things services and is extensively collected and analyzed by web-based hardware and platforms. However, issues such as service interruptions and network instability often lead to sparsely recorded trajectories, resulting in a loss of detailed movement data. As a result, recovering these trajectories to restore missing information becomes essential. Despite progress, several challenges remain unresolved. First, the lack of large-scale dense trajectory data hampers the performance of existing deep learning methods, which rely heavily on abundant data for supervised training. Second, current methods struggle to generalize across sparse trajectories with varying sampling intervals, necessitating separate re-training for each interval and increasing computational costs. Third, external factors crucial for the recovery of missing points are not fully incorporated.

To address these challenges, we propose a framework called PTR. This framework mitigates the issue of limited dense trajectory data by leveraging the capabilities of pre-trained language models (PLMs). PTR incorporates an explicit trajectory prompt and is trained on datasets with multiple sampling intervals, enabling it to generalize effectively across different intervals in sparse trajectories. To capture external factors, we introduce an implicit trajectory prompt that models road conditions, providing richer information for recovering missing points. Additionally, we present a trajectory embedder that encodes trajectory points and transforms the embeddings of both observed and missing points into a format comprehensible to PLMs. Experimental results on two public trajectory datasets with three sampling intervals demonstrate the efficacy and scalability of PTR.

1 Introduction

A trajectory is represented as a sequence of timestamped locations that depict the movement of individuals and vehicles. With the advances in web-of-things services like ride-hailing and sharing bikes and web-based platforms like Google Maps and Mapbox in

recent years, massive trajectory data is collected and analyzed. Such data plays a pivotal role in various applications, including urban planning [26], traffic management [16, 25], and personalized location services [24, 32].

Collecting trajectory data involves the coordination of multiple devices [3]. The process begins with continuously recorded GPS coordinates from devices like smartphones or IoT sensors at regular intervals. These data points are then sent to central servers or databases for storage and analysis. However, factors such as network transmission instability, device power-saving settings, and poor coverage in high-traffic or remote areas will result in the loss of trajectory points, making the collected data sparse. Such sparse trajectories failed to accurately describe movement behavior and route choices, thus limiting their effectiveness in trajectory-based applications. To mitigate this problem, it is essential to recover the missing points from sparse trajectories which improves the integrity of trajectory information. Such task is usually termed trajectory recovery.

Many works have been proposed to tackle trajectory recovery task, which can be divided into two categories: *free space trajectory recovery* [4, 6] and *map-matched trajectory recovery* [5, 27]. *Free space trajectory recovery* aims to directly restore the coordinates of missing trajectory points but cannot ensure that the recovered trajectory is constrained to the road network. Typically, an additional map-matching process is required before these trajectories can be used in navigation-based applications. *Map-matched trajectory recovery* focuses on directly recovering trajectories on the road network. In this paper, we focus on the latter setting because it can be directly utilized by downstream tasks without the need for further processing. Despite the progress made by existing methods on map-matched trajectory recovery, they still face some challenges as listed below.

1) The availability of dense trajectories is often limited. Deep learning-based trajectory recovery models are inherently data-driven, requiring a substantial number of dense trajectories as labels for supervised training. However, due to the aforementioned factors, most collected and stored trajectories are sparse, resulting in a limited availability of large-scale dense trajectory data. As a

*Both authors contributed equally to this research.

†Corresponding author.

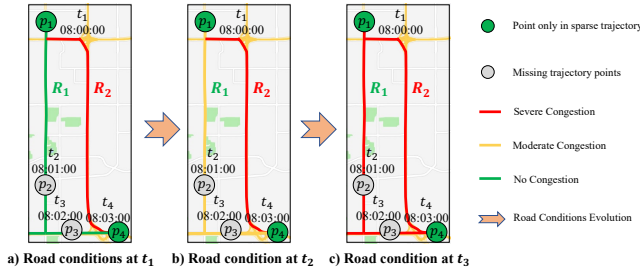


Figure 1: An example of road network evolution process.

result, the lack of sufficient dense trajectories for training makes existing deep learning models prone to overfitting and leads to diminished performance.

2) **Existing models struggle to generalize to sparse trajectories with varying sampling intervals.** Sparse trajectories often exhibit inconsistent sampling intervals due to network instability. However, most trajectory recovery models are trained on sparse trajectories with fixed sampling intervals, limiting their ability to generalize to trajectories with varying intervals. As a result, when confronted with trajectories that have different sampling intervals, these models require separate training for each interval to recover trajectories effectively, leading to significantly increased training costs.

3) **External factors related to the recovery of missing points are not incorporated.** External factors, such as road conditions, provide valuable insights that can enhance trajectory recovery. For instance, in the scenario illustrated in Figure 1, given the observed points p_1 and p_4 and the road conditions at time t_1 , it is more likely that the user took route R_1 rather than R_2 . Additionally, based on the road conditions at times t_2 and t_3 , as shown in Figures 1 (b) and (c), it becomes easier to infer that the user first accelerated and then decelerated between p_1 and p_4 . However, existing methods only consider information from the known trajectory points, overlooking the significance of external factors.

To address the aforementioned challenges, we propose a *Pre-trained Language Model for Trajectory Recovery* (PTR). By leveraging a pre-trained language model (PLM) that has been trained on large-scale corpus datasets and fine-tuning it with a limited set of dense trajectories, PTR can effectively recover trajectories even when only scarce dense trajectory data is available. PTR incorporates two key components to generalize to sparse trajectories with varying sampling intervals: first, an explicit trajectory prompt, which uses natural language to describe both the trajectory recovery task and its characteristics. This activates the PLM’s ability to recover trajectories and recognize the trajectory’s sampling interval. Second, a joint training strategy, where PTR is trained on trajectory data with multiple sampling intervals, further enhancing its generalization capabilities. To account for external factors, we introduce an implicit trajectory prompt, which integrates rich contextual information, such as road conditions, to provide insights on missing points. Lastly, we propose a trajectory embedder that encodes both observed and missing trajectory points, transforming them into representations interpretable by PLMs. This allows the PLM to capture the spatiotemporal correlations within the trajectory.

Overall, the main contributions of our work can be summarized as follows:

- We introduce PTR, a novel framework for trajectory recovery that utilizes PLMs to efficiently recover trajectories using a limited set of dense trajectories.
- We propose explicit trajectory prompts that enable the PLM to accurately interpret the trajectory recovery task and determine the sampling intervals of the trajectories. Combined with a joint training strategy on trajectories with various sampling intervals, PTR generalizes effectively to sparse trajectories across different intervals.
- We present an implicit trajectory prompt to model external factors influencing missing trajectory points and a trajectory embedder to transform the trajectory representation into a form that the PLM can process.
- We conduct extensive experiments on two real-world trajectory datasets, each with three different sampling intervals. The results show that our proposed model achieves state-of-the-art performance in both accuracy and efficiency.

2 Related Work

2.1 Free-space Trajectory Recovery

Trajectory recovery in free space aims to directly restore the GPS coordinates of missing points. Early approaches relied on predefined rules to model mobile objects [2, 20]. For example, Linear [9] assumes that vehicle movement follows uniform linear motion and employs linear interpolation for trajectory recovery. MPR [6] assumes vehicles travel along the most frequently used routes, utilizing historical trajectory data to determine route frequencies for recovery. Other studies [1, 33] use Markov models to capture spatial transitions between trajectory points. However, these methods are limited to modeling low-order transitions and struggle to capture the global spatial-temporal dependencies of trajectories.

Recent deep learning-based approaches have provided more effective solutions for trajectory recovery [29, 30]. DHTR [23] employs a GRU-based seq2seq model to analyze user route transitions, integrating Kalman filtering to improve recovery accuracy. Attn-Move [28] uses attention mechanisms and LSTM to capture overall human movement preferences. PeriodicMove [21] models each user trajectory as a graph, employing graph neural networks to efficiently capture user preferences by leveraging historical route transitions. TERI [4] introduces a two-stage framework based on transformers to recover trajectories with unequal spacing, while TrajBERT [19] utilizes the BERT [7] framework to recover implicit trajectories, focusing on coarser-grained outputs such as area or Wi-Fi IDs. Although these methods show promising results, they require an additional map-matching process to align the recovered trajectories with the road network before they can be applied in navigation systems. This two-stage process leads to error accumulation and introduces significant time overhead, as the map-matching step is time-consuming.

2.2 Map-matched Trajectory Recovery

Compared with the above methods, map-matched trajectory recovery incorporates the road network as input and aims to recover the trajectory directly onto the road. To this end, MTrajRec [17] first

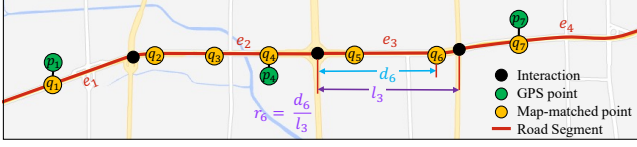


Figure 2: An illustration of map-matched trajectory, road segment e , and moving ratio r .

represents the trajectory point with a road segment and moving rate, utilizing the seq2seq-based multi-task framework to capture the spatiotemporal correlations within the trajectory. Following this idea, RNTrajRec [5] further models the relationship between trajectories and road networks, designing a spatial-temporal transformer architecture to encode sparse trajectories. MM-STGED [27] models sparse trajectories from a graph perspective, considering both micro and macro semantic information of trajectories.

Although these methods demonstrate promising progress in trajectory recovery, their performance are still hindered by the poor availability of large-scale dense trajectories and limited in generalization to different sampling intervals discussed in Section 1.

3 Preliminaries

3.1 Definitions

Definition 3.1 (Trajectory). A trajectory is defined as a series of timestamped locations, denoted as $\mathcal{T} = \langle p_1, \dots, p_{|\mathcal{T}|} \rangle$ where $p_i = (lat_i, lng_i, t_i)$ represents the latitude and longitude coordinates of an object at the time $t_i, i \in \{1, \dots, |\mathcal{T}|\}$. $|\mathcal{T}|$ is the length of trajectory. The sampling interval of the trajectory \mathcal{T} is $t_i - t_{i-1}, i \in \{2, \dots, |\mathcal{T}|\}$.

Definition 3.2 (Road Network). A road network is defined as a directed graph $\mathcal{G} = (\mathcal{V}, \mathcal{E})$, where \mathcal{V} denotes the set of nodes. Each node $v \in \mathcal{V}$ signifies an intersection that links various road segments, and each node possesses attributes of latitude and longitude. \mathcal{E} represents the set of edges, where each edge $e \in \mathcal{E}$ denotes road segment that connecting two intersections. An edge can be characterized by its starting intersection $e.start \in \mathcal{V}$ and ending intersection $e.end \in \mathcal{V}$.

Definition 3.3 (Map-matched Trajectory). By employing the map-matching algorithm, a trajectory \mathcal{T} can be projected onto the road network and return the map-matched trajectory \mathcal{T}_m . As a result, each point of the map-matched trajectory aligns accurately with a particular road. The map-matched trajectory is represented as $\mathcal{T}_m = \langle q_1, \dots, q_{|\mathcal{T}_m|} \rangle$, where each $q_j = (e_j, r_j, t_j)$ signifies the vehicle’s location at time $t_j, j \in \{1, \dots, |\mathcal{T}_m|\}$. Here, $e \in \mathcal{V}$ is the matched road segment, and r is the moving ratio, which quantifies the proportion of the distance traveled from the starting point of a road segment in relation to the total length of that road segment.

Example 3.4. Figure 2 gives an example of a map-matched trajectory. For a sparse trajectory $\mathcal{T}_s = \langle p_1, p_4, p_7 \rangle$ with the sampling interval of 90 seconds, its corresponding dense map-matched trajectory is represented by $\mathcal{T}_m = \langle q_1, \dots, q_7 \rangle$ with a sampling interval of 30 seconds. Take a matching point q_6 as an example. It falls on the road e_3 , so its road segment is e_3 . The distance of q_6 from the

start point of the road is represented as d_6 , while the total length of e_3 is denoted by l_3 . Therefore, the moving ratio r_6 can be calculated as $r_6 = \frac{d_6}{l_3}$.

3.2 Problem Statement

Map-matched Trajectory Recovery. Given a sparse trajectory $\mathcal{T}_s = \langle p_1, \dots, p_{|\mathcal{T}_s|} \rangle$ with a sampling interval of μ . The goal of map-matched trajectory recovery is to reconstruct the dense map-matched trajectory $\mathcal{T}_m = \langle q_1, \dots, q_{|\mathcal{T}_m|} \rangle$ with a sampling interval of ϵ . Note that the sampling interval μ is larger than ϵ .

4 Methodology

4.1 Overall Pipeline

In this paper, we present PTR, which fine-tunes a PLM pre-trained on a large-scale corpus to efficiently recover trajectories with limited dense data. The framework of PTR, shown in Figure 3, comprises three main components: trajectory prompts, a trajectory embedder, and a PLM-based trajectory encoder.

Trajectory prompts offer essential information from two key components. First, explicit trajectory prompts, expressed in natural language, outline the trajectory recovery task and key trajectory characteristics. These prompts activate the PLM’s ability to recover trajectories and identify varying sampling intervals in sparse trajectories. With joint training on trajectories across different intervals, PTR achieves robust generalization. Second, implicit trajectory prompts model road conditions, providing crucial external factors of missing points.

The trajectory embedder effectively enhances the PLM’s understanding of trajectories. It begins by normalizing sparse trajectories with varying sampling intervals μ into a uniform interval ϵ . Next, each trajectory point, including both observed and missing points, is encoded into an embedding that captures both local and global semantics. Finally, the embedding is transformed into a format understood with the PLM.

In the PLM-based trajectory encoder, most of the encoder’s parameters are frozen to preserve the pre-trained knowledge, while the multi-head attention layer remains trainable, allowing the model to capture the spatiotemporal correlations within the trajectory. Finally, the output layer predicts the road segment e and the moving ratio r for the recovered map-matched trajectory at each step.

4.2 Trajectory Prompts

To enable PLMs to recover trajectories with different intervals and efficiently model external factors for missing trajectory points, we introduce explicit and implicit trajectory prompts.

4.2.1 Explicit Trajectory Prompt. The explicit trajectory prompt offers a structured textual description at both the task and trajectory levels, enabling PTR to adapt to varying sampling intervals. At the task level, it includes the following components:

- **<Task Part>**: Sparse trajectory recovery.
- **<Target Part>**: Output the road segment and moving ratio for each point in the trajectory.

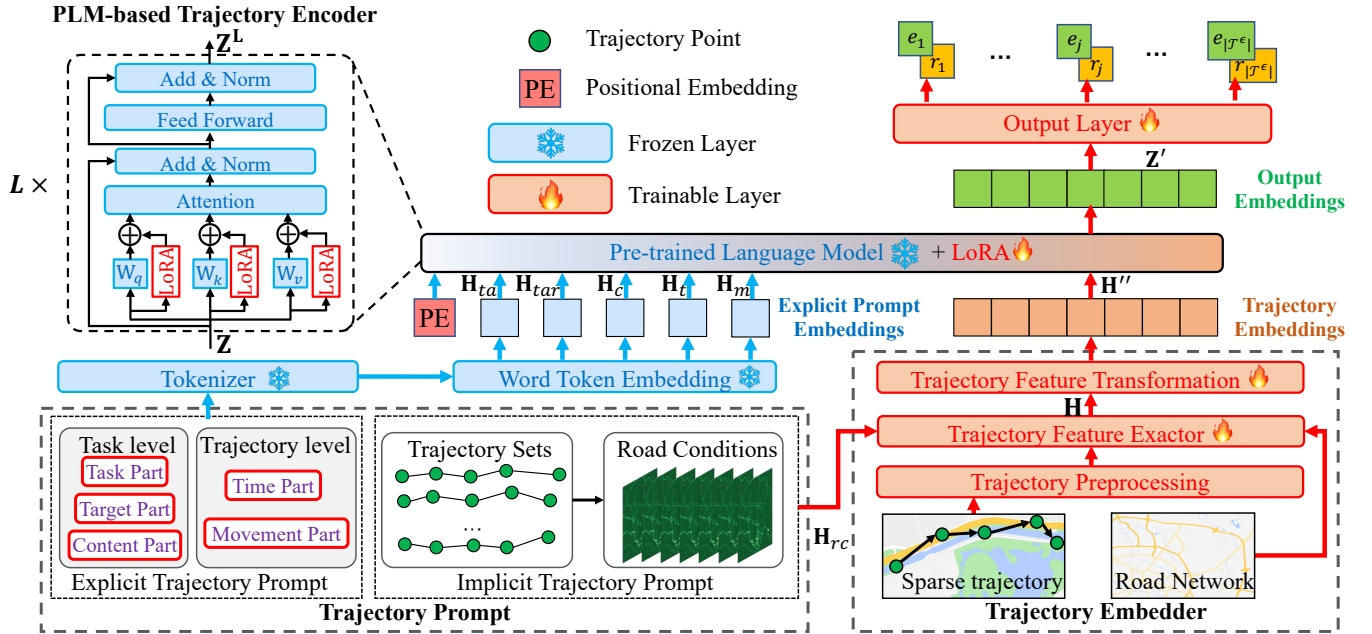


Figure 3: The framework of PTR, consists of Trajectory Prompt, Trajectory Embedder, and PLM-based Trajectory Encoder.

- **<Content Part>**: The sparse trajectory is sampled every $\{large\ sampling\ interval\}$ and aims to recover trajectory every $\{small\ sampling\ interval\}$ seconds.

The content within the placeholders $\{\}$ is filled with trajectory-specific information. All trajectories share the same task-level prompt. The **<Task Part>** informs the PLM about the overall task to be performed, the **<Target Part>** defines the required output format, and the **<Content Part>** specifies the sampling intervals, guiding the PLM in effectively analyzing the trajectories.

At the trajectory level, the explicit trajectory prompt provides detailed characteristics of the trajectory, consisting of:

- **<Time Part>**: The trajectory started at $\{start\ time\}$ on $\{day-in-week\}$ and ended at $\{end\ time\}$ on $\{day-in-week\}$.
- **<Movement Part>**: Total time cost: $\{x\ minutes\ y\ seconds\}$. Total space transfer distance: $\{z\ kilometers\}$.

The **<Time Part>** provides the trajectory’s specific start and end times, helping the PLM understand the duration and potential time patterns, such as morning or evening peaks. The **<Movement Part>** supports the PLM in inferring the trajectory’s movement.

After obtaining the prompt for each part, we use the tokenizer and word token embedding in PLMs to convert text into embeddings. The embedding of **<Task Part>**, **<Target Part>**, **<Content Part>**, **<Time Part>**, and **<Movement Part>** are denoted by \mathbf{H}_{ta} , \mathbf{H}_{tar} , \mathbf{H}_c , \mathbf{H}_t , and \mathbf{H}_m . These embeddings are then concatenated to form the overall explicit trajectory prompt embedding.

$$\mathbf{H}^e = \mathbf{H}_{ta} || \mathbf{H}_{tar} || \mathbf{H}_c || \mathbf{H}_t || \mathbf{H}_m, \quad (1)$$

where $||$ is the concatenate operation.

4.2.2 Implicit Trajectory Prompt. We incorporate road conditions as external factors for missing trajectory points, as they provide

insights into both the surrounding environment and the object’s movement, which are all helpful for trajectory recovery. For instance, vehicles typically slow down in congested areas and accelerate in less congested regions. Given the complexity and variability of real-world road conditions, which are difficult to express in natural language, we represent them as an implicit trajectory prompt.

To obtain the road conditions for each trajectory point, we first calculate the average road conditions across all areas and time intervals, then extract the relevant information for each point. Specifically, we divide the area of interest into a spatial grid of $I \times J$ cells and partition the time into T slices. For each grid cell, we compute the total traffic, resulting in a regional flow matrix $\mathbf{RC} \in \mathbb{R}^{I \times J \times T}$. To capture the spatiotemporal correlations among different regions, we apply a 2D convolution (2D CNN) along the spatial dimensions and a 1D CNN along the temporal dimension, yielding the road condition representation $\mathbf{H}_{rc} \in \mathbb{R}^{I \times J \times T \times F}$, where F is the number of features. Formally:

$$\mathbf{H}_{rc} = \text{Conv1d}(\text{Conv2d}(\mathbf{RC})) \in \mathbb{R}^{I \times J \times T \times F} \quad (2)$$

Obviously, the road conditions of a trajectory point are indexed by its longitude, latitude, and timestamp. However, it is challenging for missing points as their geographic coordinates are unknown. To address this, we introduce a road condition diffusion strategy that approximates the missing conditions using neighboring traffic. The implementation details will be elaborated in Section 4.3.2.

4.3 Trajectory Embedder

To efficiently encode trajectory points and enable PLMs to better understand them, we introduce the trajectory embedder.

4.3.1 Trajectory Preprocessing Layer. For different sparse trajectories, their sampling intervals μ are not constant, such as 4 minutes,

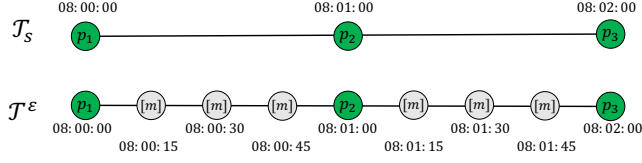


Figure 4: An illustration of trajectory preprocessing layer.

2 minutes, or 1 minute. To convert these into a uniform sampling interval, we introduce a placeholder ‘[m]’ to mark missing trajectory points and generate a preprocessed sparse trajectory \mathcal{T}^ϵ , where the length of $|\mathcal{T}^\epsilon| = \frac{p_{|T_s|}.t - p_1.t}{\epsilon}$. Although the location of ‘[m]’ is unknown, its timestamp can still be calculated, as illustrated in Figure 4.

4.3.2 Trajectory Feature Extractor. To embed trajectory points, we propose the trajectory feature extractor. Given the preprocessed sparse trajectory \mathcal{T}^ϵ , there are two cases for its trajectory point characteristics:

- Case 1: the trajectory point $s \in \mathcal{T}^\epsilon$ is observed. i.e., $\exists k \in \{1, \dots, |\mathcal{T}^\epsilon|\}, p_k.t = s.t$.
- Case 2: the location of trajectory point $s \in \mathcal{T}^\epsilon$ is missing. i.e., $s = [m]$, note that its time $s.t$ is known.

For case 1, we use Learnable Fourier Features [13, 22] to encode the continuous latitude and longitude of s into an F -dimensional vector using the feature mapping function $\Phi(x) : \mathbb{R} \rightarrow \mathbb{R}^F$. Formally:

$$\Phi(x) = W_\Phi [\cos x W_r \parallel \sin x W_r], \quad (3)$$

where $W_r \in \mathbb{R}^{F/2}$ and $W_\Phi \in \mathbb{R}^{F \times F}$ represent the learnable parameters, and $x \in \{s.lat, s.lon\}$.

Using the feature mapping function $\Phi(\cdot)$, the relative information between points x and y can be captured through multiplication operations. This relative information helps infer crucial details like the distance between trajectory points, which is important for understanding movement. For instance, a larger distance between two points may indicate a higher likelihood of vehicle acceleration.

Additionally, considering that vehicles move within the road network, the relationship between a trajectory point and its surrounding road segments is critical. To measure the relationship between a trajectory point s and a road segment l , we define a function $f(d_{s,l})$ based on their shortest distance:

$$f(d_{s,l}) = \begin{cases} e^{-\left(\frac{d_{s,l}}{\kappa}\right)^2} & \text{if } d_{s,l} < \varphi_{dist}, \\ 0 & \text{otherwise,} \end{cases} \quad (4)$$

where $d_{s,l}$ is the shortest distance between s and road l , κ is a hyperparameter, and φ_{dist} is a distance threshold. Then, we obtain the road network representation $\mathbf{h}_s^{\text{road}}$ by:

$$\mathbf{h}_s^{\text{road}} = \frac{\sum_{l=1}^{|\mathcal{V}|} f(d_{s,l}) * \mathbf{M}_l}{\sum_{l=1}^{|\mathcal{V}|} f(d_{s,l})}, \quad (5)$$

where $\mathbf{M}_l \in \mathbb{R}^F$ is the learnable embedding of road segment l , and $|\mathcal{V}|$ is the total number of road segments. Finally, the complete

representation of a trajectory point s is obtained as:

$$\mathbf{h}_s = W_1 [(\Phi(s.lat) + \Phi(s.lon)) \parallel \mathbf{h}_s^{\text{road}}] + b_1, \quad (6)$$

where $W_1 \in \mathbb{R}^{2F \times F}$ and $b_1 \in \mathbb{R}^F$ is the learnable parameters.

For case 2, where the location of point s is unknown, here we use road conditions to represent its features, as described in Section 4.2.2. Since the road conditions at a specific point are influenced by the surrounding conditions, which propagate along both temporal and spatial dimensions, we propose a road condition diffusion strategy to model the road conditions of the missing location.

First, for the missing point s , we identify the observed forward and backward trajectory points, s_f and s_b , respectively. For instance, in Figure 4, suppose we have a missing point s timestamped at 8:00:45, its observed forward point $s_f = p_1$ and the backward point $s_b = p_2$. Then, we retrieve the road conditions of s_f and s_b as follows:

$$\begin{aligned} \mathbf{h}_{rc}^f &= \mathbf{H}_{rc} [\pi_{lat}(s_f.lat), \pi_{lng}(s_f.lng), \pi_t(s_f.t)], \\ \mathbf{h}_{rc}^b &= \mathbf{H}_{rc} [\pi_{lat}(s_b.lat), \pi_{lng}(s_b.lng), \pi_t(s_b.t)], \end{aligned} \quad (7)$$

where π_{lat} , π_{lng} , and π_t are index functions mapping latitude, longitude, and time to their respective indices. Next, we calculate the time interval between s and s_f and s_b , denoted as $\Delta t_f = s.t - s_f.t$ and $\Delta t_b = s_b.t - s.t$. The road condition of point s is then computed as:

$$\mathbf{h}_{rc}^s = \frac{e^{-\Delta t_f} \mathbf{h}_{rc}^f + e^{-\Delta t_b} \mathbf{h}_{rc}^b}{e^{-\Delta t_f} + e^{-\Delta t_b}} \quad (8)$$

In addition, we encode the time intervals Δt_f and Δt_b to quantify the relative position of s . The final representation of s is given by:

$$\begin{aligned} \mathbf{h}_s &= W_2 [\mathbf{m} \parallel \text{FC}(\Delta t_f \parallel \Delta t_b) \parallel \mathbf{h}_{rc}^s] + b_2, \\ \text{FC}(\cdot) : \mathbb{R}^2 &\rightarrow \mathbb{R}^F, \end{aligned} \quad (9)$$

where $\mathbf{m} \in \mathbb{R}^F$ is a learnable vector to represent the location is missing, and $\text{FC}(\cdot)$ is the fully connection layer. $W_2 \in \mathbb{R}^{3F \times F}$ and $b_2 \in \mathbb{R}^F$ are the learnable parameters. Finally, the overall trajectory representation is $\mathbf{H} \in \mathbb{R}^{|\mathcal{T}^\epsilon| \times F}$.

4.3.3 Trajectory Feature Transformation. To enhance the model’s ability to comprehend trajectory features, we introduce K reference tokens $\mathbf{E}_w \in \mathbb{R}^{K \times F}$, inspired by [8, 11], to bridge the connection between PLMs and the trajectory. These reference tokens are designed to capture the global semantics of the trajectory.

Given the trajectory embedding \mathbf{H} , we first apply a 1D CNN to aggregate neighboring information and capture local movement patterns:

$$\mathbf{H}' = \text{Conv1d}(\mathbf{H}) \quad (10)$$

Next, we compute self-attention between the trajectory embedding \mathbf{H}' and the reference tokens \mathbf{E}_w to capture the global semantics, where \mathbf{H}' acts as the query, and \mathbf{E}_w as both the key and value:

$$\mathbf{H}'' = \text{Attention}(\mathbf{H}', \mathbf{E}_w, \mathbf{E}_w) \quad (11)$$

After transforming the embedding \mathbf{H}'' in the token space, we concatenate it with the explicit trajectory prompt embedding \mathbf{H}^e to form the final trajectory representation:

$$\mathbf{Z} = \mathbf{H}^e \parallel \mathbf{H}'' \quad (12)$$

Then, we add the Transformer positional embedding PE in each element of \mathbf{Z} and feed it into PLMs encoder to encode trajectory.

4.4 PLM-based Trajectory Encoder

As shown in Figure 3, we use the stacked Transformer layers as the fundamental architecture of PLMs. To make PLMs fully adaptable to the trajectory recovery task, we employ the Low-Rank Adaptation (LoRA) algorithm [10]. LoRA introduces additional parameters within the Transformer block, reducing the number of trainable parameters and computational complexity while enhancing the PLM’s performance on new tasks.

Specifically, in each self-attention block of the Transformer, we introduce additional weights $\Delta\mathbf{W}_q \in \mathbb{R}^{F \times F}$, $\Delta\mathbf{W}_k \in \mathbb{R}^{F \times F}$, and $\Delta\mathbf{W}_v \in \mathbb{R}^{F \times F}$ for the query, key, and value matrices \mathbf{W}_q , \mathbf{W}_k , and \mathbf{W}_v . To reduce the parameter count, the additional weights $\Delta\mathbf{W}$ are decomposed into two low-rank matrices, $\mathbf{B} \in \mathbb{R}^{F \times r}$ and $\mathbf{C} \in \mathbb{R}^{r \times F}$, where $r \ll F$. The modified query, key, and value matrices in each self-attention block are updated as $\mathbf{W}_q = \mathbf{W}_q + \Delta\mathbf{W}_q$, $\mathbf{W}_k = \mathbf{W}_k + \Delta\mathbf{W}_k$, and $\mathbf{W}_v = \mathbf{W}_v + \Delta\mathbf{W}_v$. Formally, the output of the l -th transformer layer is defined as:

$$\mathbf{Z}^l = \text{LoRA}(\text{Transformer}(\mathbf{Z}^{l-1})) \quad (13)$$

After stacking L Transformer layers, we discard the explicit trajectory prompt portion and obtain the output embeddings $\mathbf{Z}' \in \mathbb{R}^{|\mathcal{T}^\epsilon| \times d}$.

For the j -th element of \mathbf{Z}' , we apply the softmax function to calculate the probability of each road segment and use the argmax function to return the predicted road segment e_j . We employ a MLP with a Sigmoid activation function to determine the moving ratio r_j .

4.5 Training

4.5.1 Loss Function. We use multi-task learning to simultaneously optimize road segment recovery and moving ratio recovery tasks. For the road segment recovery, we use the cross-entropy as the loss function:

$$\mathcal{L}_e = -\frac{1}{|\mathcal{T}^\epsilon|} \sum_{j=1}^{|\mathcal{T}^\epsilon|} \log(\hat{e}_j | \mathbf{Z}'_j) \quad (14)$$

For the moving ratio, we use the mean squared error as the loss function:

$$\mathcal{L}_r = \frac{1}{|\mathcal{T}^\epsilon|} \sum_{j=1}^{|\mathcal{T}^\epsilon|} |r_j - \hat{r}_j|^2 \quad (15)$$

The final loss function is $\mathcal{L} = \mathcal{L}_e + \lambda\mathcal{L}_r$, where λ is a hyper-parameter to balance two tasks.

4.5.2 Training Strategy. To generalize PTR in recovering sparse trajectories with various sampling intervals, we propose the following training approach.

For the dense trajectory dataset \mathbb{T} , which is set as a 15-second sampling interval in our experiments. To create sparse trajectory datasets, we re-sample \mathbb{T} at three different intervals: 1 minute, 2 minutes, and 4 minutes, resulting in three datasets: \mathbb{T}_1 , \mathbb{T}_2 , and \mathbb{T}_4 . These are then combined to form a larger training dataset, \mathbb{T}_{all} .

$$\mathbb{T}_{all} = \mathbb{T}_1 \cup \mathbb{T}_2 \cup \mathbb{T}_4. \quad (16)$$

By training PTR on \mathbb{T}_{all} , we achieve balanced performance across the different sampling intervals. Subsequently, we fine-tune the

model on each individual sparse trajectory dataset to further improve trajectory recovery performance.

5 Experiments

In this section, we present comprehensive experiments to evaluate the effectiveness of PTR on two real-world trajectory datasets with three different sparse trajectory sampling intervals. These experiments are designed to answer the following key questions:

- **RQ1:** How does PTR’s performance compare to other baseline methods across different sampling intervals of sparse trajectories?
- **RQ2:** How well does PTR perform when trained with limited data?
- **RQ3:** What is the contribution of each component in PTR to the overall model performance?

5.1 Datasets

We assess our model using two publicly available trajectory datasets from Chengdu, China, and Porto, Portugal. The Chengdu dataset¹ contains trajectory data collected in November 2016. The Porto dataset² includes trajectory from 442 taxis, collected from July 2013 to June 2014. Both datasets are standardized to a sampling interval of 15 seconds. We remove trajectories with travel times less than 5 minutes or exceeding 1 hour, as well as outlier trajectories. The road network data is obtained from the OpenStreetMap website³. We employ a map-matching algorithm [14] to project the trajectory onto the road network and obtain the ground truth of the road segments and moving rates. The detailed overview of the dataset characteristics is provided in Table 4.

5.2 Baselines

To evaluate the effectiveness of our model, we compare PTR with ten baseline methods. These include five free space trajectory recovery models: **HMM** [14] + **ShortestPath**, **Linear** [9] + **HMM** [14], **MPR** [6] + **HMM** [14], **DHTR** [23] + **HMM** [14], and **Attn-Move** [28] + **Rule**, as well as five map-matched trajectory recovery models: **MTrajRec** [17], **T2vec** [12] + **Decoder**, **T3s** [31] + **Decoder**, **RNTrajRec** [5], and **MM-STGED** [27]. The details of each baseline are provided in Appendix B.

5.3 Evaluation Metrics

We employ five common metrics to assess the effectiveness of our model followed [5, 17, 27]. For road segment recovery, we utilize **Accuracy (Acc)**, **Recall**, and **Precision (Prec)** metrics to evaluate. A higher result indicates a more precise road segment recovery. And employ **Mean Absolute Error (MAE)** and the **Root Mean Square Error (RMSE)** in assessing the recovered GPS coordinates. Lower values of these metrics indicate a higher level of accuracy in the recovery results. The details of each metric are provided in Appendix C.

¹<https://outreach.didichuxing.com/>

²<https://www.kaggle.com/competitions/pkdd-15-predict-taxi-service-trajectory-i/data>

³<http://www.openstreetmap.org/>

Table 1: Performance comparison on two datasets with sampling intervals at 4 minutes, 2 minutes, and 1 minute, respectively. The best results are highlighted in bold, while the underline indicates the second-best results.

Sampling Interval	Methods	Chengdu					Porto				
		Acc(%)	Recall(%)	Prec(%)	MAE	RMSE	Acc(%)	Recall(%)	Prec(%)	MAE	RMSE
$\mu = 4$ minutes $\rightarrow \epsilon = 15$ seconds	HMM + ShortestPath	26.85	28.64	29.55	939.3	1047.7	20.19	26.22	33.51	886.9	941.5
	Linear + HMM	26.42	30.45	36.15	974.5	1145.4	32.23	36.09	49.80	489.3	637.3
	MPR + HMM	36.93	38.62	44.53	821.9	914.1	32.22	38.67	48.07	534.0	700.2
	DHTR + HMM	41.48	57.34	50.48	673.6	911.3	32.02	58.29	45.61	456.7	627.1
	AttnMove + Rule	63.43	73.97	78.72	358.2	916.7	49.31	48.62	78.03	310.0	621.3
	MTrajRec	65.79	75.14	78.42	315.1	904.4	52.36	60.39	77.28	266.1	590.1
	T3s + Decoder	65.60	75.26	78.14	318.2	926.3	52.24	60.24	77.80	270.4	594.9
	T2vec + Decoder	66.51	75.68	78.27	307.5	915.2	53.13	60.27	77.62	256.3	571.0
	RNTrajRec	67.66	75.59	79.97	306.1	886.0	54.59	60.42	79.20	248.1	549.1
	MM-STGED	70.64	76.04	81.63	266.2	829.7	57.30	59.48	80.21	222.8	510.4
	PTR	74.12	79.63	86.46	262.8	483.0	57.61	59.15	82.19	200.9	376.9
PTR + FT	74.58	80.09	86.63	253.2	465.7	57.67	59.08	<u>82.05</u>	200.8	370.2	
$\mu = 2$ minutes $\rightarrow \epsilon = 15$ seconds	HMM + ShortestPath	33.85	47.89	48.31	754.1	826.2	27.30	40.05	46.00	647.3	747.0
	Linear + HMM	43.78	45.35	48.77	816.9	1054.7	49.35	50.45	63.87	408.7	609.8
	MPR + HMM	49.88	54.62	50.94	474.8	899.0	49.76	52.97	62.86	409.8	610.9
	DHTR + HMM	47.17	60.16	51.73	662.0	912.2	43.76	65.25	52.10	385.3	578.0
	AttnMove + Rule	71.98	77.42	80.67	291.1	764.8	61.39	60.90	82.98	213.4	468.5
	MTrajRec	74.52	78.25	81.09	254.5	885.7	61.65	65.65	78.99	179.9	451.5
	T3s + Decoder	74.62	78.95	81.79	242.2	857.5	61.75	65.53	79.14	181.3	461.2
	T2vec + Decoder	75.69	78.86	81.68	231.6	783.6	62.24	65.77	78.97	173.9	438.0
	RNTrajRec	75.80	79.35	81.86	218.5	757.0	63.39	65.84	79.25	171.3	433.9
	MM-STGED	78.14	80.06	83.58	197.2	696.0	65.69	66.15	80.74	152.5	400.8
	PTR	81.76	84.31	88.38	187.4	366.2	66.40	66.52	82.14	141.9	294.6
PTR + FT	82.29	84.59	88.72	181.2	349.0	66.72	66.87	82.38	141.7	293.5	
$\mu = 1$ minute $\rightarrow \epsilon = 15$ seconds	HMM + ShortestPath	35.92	67.92	60.16	529.7	638.2	34.75	48.46	48.67	527.2	659.3
	Linear + HMM	68.59	65.66	66.67	707.4	1005.2	66.17	64.72	75.22	368.3	571.1
	MPR + HMM	62.25	62.67	60.53	418.8	659.0	66.27	65.66	74.51	402.6	628.2
	DHTR + HMM	51.09	63.40	50.14	584.7	750.4	52.98	69.60	57.17	420.4	625.8
	AttnMove + Rule	79.60	81.55	82.75	194.4	752.6	72.07	69.59	80.41	156.6	360.7
	MTrajRec	81.12	81.73	83.75	187.1	718.4	71.65	70.92	80.35	114.9	332.3
	T3s + Decoder	80.90	82.78	83.15	187.1	713.0	71.78	71.61	80.16	110.1	328.0
	T2vec + Decoder	81.69	81.90	83.88	185.6	714.1	71.86	71.10	80.48	114.2	334.7
	RNTrajRec	81.88	82.09	84.84	177.9	702.5	72.31	71.88	80.57	110.3	325.7
	MM-STGED	84.26	84.15	85.92	154.0	633.5	73.16	72.27	80.81	108.2	321.9
	PTR	87.17	87.99	90.52	141.4	290.8	<u>74.42</u>	<u>72.78</u>	<u>82.82</u>	95.6	211.7
PTR + FT	88.15	88.82	91.04	138.6	289.1	75.35	73.87	83.28	95.2	<u>220.3</u>	

5.4 Settings

We split the trajectory dataset into training, validation, and testing sets in a 7:2:1 ratio. Following previous work [5, 17, 27], for dense map-matched trajectories, we set the sampling interval $\epsilon = 15$ seconds. To generate sparse trajectories, for each dense trajectory, we retain the first and last points and create three sparse versions by setting the sampling intervals $\mu = 4$ minutes, 2 minutes, and 1 minute, respectively.

During training, we integrate sparse trajectories with three different sampling intervals to train PTR. After training, we evaluate its performance in recovering trajectories across various sampling intervals to assess its generalizability. To further enhance performance, we fine-tune the trained model for each specific sampling interval, allowing for a more precise recovery.

We employ PyTorch [15] framework to implement PTR, with a learning rate of $1e-4$ and a batch size of 64. BERT [7] is selected as the foundation model for PLMs, as its encoder-only structure is well-suited to the reconstruction task due to its effective use of bi-directional contextual information from the trajectory [18]. For road condition extraction, the area of interest is divided into a 64×64 grid, and the time dimension is partitioned into hourly intervals. The hidden state dimension is set to $F = 512$. In Equation 4, we set

$\kappa = 15$ and $\varphi_{dist} = 50$ meters. The model is trained for 50 epochs with early stopping, using a patience of 10 epochs. All experiments are conducted on NVIDIA RTX A4000 GPUs.

5.5 Experimental Results (RQ1)

Table 1 reports a comparison of the results between our model and the baselines across various sampling intervals of sparse trajectories on both the Chengdu and Porto datasets. As the sampling interval increases, the map-matched trajectory recovery task is more difficult. Due to the more complex road network structure in Porto compared to Chengdu, with Porto having 100.9 roads / km^2 and Chengdu having 38.1 roads / km^2 , the accuracy of road segment recovery is lesser in Porto than in Chengdu.

Compared to other baselines, our model achieves superior performance across all metrics, with an average improvement of 16.51% on the Chengdu dataset and 9.35% on the Porto dataset. Notably, it shows substantial gains in RMSE metrics, with an average reduction of 351.8 meters in Chengdu and 119.2 meters in Porto. This indicates PTR generalizes effectively, enabling it to accurately recover trajectories with varying sampling intervals. By fine-tuning at the specific sampling interval, **PTR + FT**, our model further improves Acc by 1.72% and 0.32%. These outstanding results can be attributed

Table 2: Scalability analysis on Chengdu dataset.

Sampling Interval	Rate Metric	20%		40%		60%		80%		100%	
		Acc(%)	RMSE	Acc(%)	RMSE	Acc(%)	RMSE	Acc(%)	RMSE	Acc(%)	RMSE
$\mu = 4$ minutes $\rightarrow \epsilon = 15$ seconds	MTrajRec	60.73	1048.0	63.58	968.5	64.73	929.4	65.39	914.6	65.79	904.4
	T3s + Decoder	60.49	1098.9	63.32	968.7	64.23	961.9	65.04	942.3	65.60	926.3
	T2vec + Decoder	62.17	966.1	64.92	946.1	64.95	972.3	65.31	946.8	66.51	915.2
	RNTrajRec	60.80	998.0	62.85	931.3	64.19	909.1	65.46	835.0	67.66	886.0
	MM-STGED	64.61	935.0	67.76	881.8	68.53	853.7	69.95	825.3	70.64	829.7
	PTR	68.30	585.3	71.57	515.6	72.74	512.5	73.56	488.3	74.12	483.0
$\mu = 2$ minutes $\rightarrow \epsilon = 15$ seconds	MTrajRec	69.85	919.8	72.58	907.4	73.97	902.3	74.32	891.3	74.52	885.7
	T3s + Decoder	68.86	909.5	72.29	897.2	73.63	883.8	74.53	868.8	74.62	857.5
	T2vec + Decoder	69.47	905.4	72.77	858.3	73.80	855.8	74.89	831.3	75.69	783.6
	RNTrajRec	68.05	991.0	70.20	856.9	71.17	834.4	72.62	795.3	75.80	757.0
	MM-STGED	71.65	865.0	75.32	773.0	75.49	752.1	76.94	747.7	78.14	696.0
	PTR	76.29	452.8	79.37	411.5	80.37	395.4	81.18	377.4	81.76	366.2
$\mu = 1$ minute $\rightarrow \epsilon = 15$ seconds	MTrajRec	75.39	937.5	78.53	835.1	80.01	794.3	80.93	725.7	81.12	718.4
	T3s + Decoder	76.49	917.1	79.08	824.9	80.65	767.8	80.82	716.5	80.90	713.0
	T2vec + Decoder	75.89	845.4	79.09	746.8	79.41	752.3	81.21	742.2	81.69	714.1
	RNTrajRec	75.65	846.2	79.48	784.8	79.61	769.3	81.74	742.5	81.88	702.5
	MM-STGED	76.02	857.7	79.86	734.7	82.25	676.4	83.44	663.0	84.26	633.5
	PTR	81.62	397.5	84.59	352.0	85.75	328.7	86.73	305.4	87.17	290.8

to the strong generalization capability of the PLM in processing sparse trajectories with varying sampling intervals. Additionally, the trajectory embedder plays a pivotal role in connecting trajectory data with the PLM, efficiently capturing spatial-temporal correlations and converting trajectory embeddings into a format that the PLM can effectively process and understand.

We also analyze the convergence rate of PTR across different sampling intervals, as shown in Figure 5 and 6. It demonstrates rapid convergence within just a few epochs on both the Chengdu and Porto datasets. While fine-tuning enhances performance further, the model stabilizes by the 3th epoch, indicating that PTR can deliver satisfactory results within a short training period.

5.6 Scalability Analysis (RQ2)

To evaluate the effectiveness of PTR in trajectory recovery when dense trajectory data is limited, we conduct scalability experiments on the Chengdu dataset. Specifically, we train the model using subsets of the training set at 20%, 40%, 60%, 80%, and 100%, and evaluate performance on the test set. The results are presented in Table 2.

As the size of the training set increases, we observe performance improvements across all baseline models. Notably, with only 20% of the training data, PTR already surpasses most baselines, trailing only MM-STGED. With 40% of the training data, PTR outperforms all other models, demonstrating its strong generalization ability. This advantage underscores the practicality of PTR in real-world scenarios, where obtaining large-scale dense trajectory data is often challenging.

5.7 Ablation Study (RQ3)

To evaluate the effects of various components in PTR, we conduct ablation experiments on the Chengdu and Porto datasets with sampling intervals of 2 minutes. We compare PTR with the following five variants.

- **w/o explicit trajectory prompt:** We remove the explicit trajectory prompt.

Table 3: Ablation study on two datasets with sampling intervals at 2 minutes.

Datasets	Methods	Acc(%)	Recall(%)	Prec(%)	MAE	RMSE
Chengdu	w/o explicit trajectory prompt	81.04	84.08	88.07	205.8	394.2
	w/o implicit trajectory prompt	81.43	84.28	88.14	191.4	371.1
	w/o trajectory prompt	80.70	83.61	87.73	225.9	407.4
	w/o road network	81.28	84.22	88.04	194.5	375.6
	w/o reference tokens	80.83	83.36	86.68	236.6	437.2
	PTR	81.76	84.31	88.38	187.4	366.2
Porto	w/o explicit trajectory prompt	66.13	66.19	81.98	157.9	314.6
	w/o implicit trajectory prompt	66.18	66.22	82.01	149.6	298.1
	w/o trajectory prompt	65.52	65.89	81.51	171.0	339.4
	w/o road network	66.11	66.27	81.90	150.7	302.8
	w/o reference tokens	65.89	65.07	80.57	165.4	327.7
	PTR	66.40	66.52	82.14	141.9	294.6

- **w/o implicit trajectory prompt:** We use the ‘[MASK]’ token in the BERT to represent the missing location.
- **w/o trajectory prompt:** We remove both the explicit and implicit trajectory prompt, and the missing points are represented by the ‘[MASK]’ token in BERT.
- **w/o road network:** We only use the Learnable Fourier Feature for encoding the observed trajectory points while removing the road network feature.
- **w/o reference tokens:** We remove the trajectory feature transformation layer in the trajectory embedder module.

As shown in Table 3, each component of PTR is essential. The explicit trajectory prompt provides task and trajectory-related textual information, enabling PLMs to effectively understand the trajectory recovery tasks. Omitting this component leads to a performance decrease. When the implicit trajectory prompt is removed, many missing locations are replaced by the ‘[MASK]’ token in BERT, limiting the model’s ability to capture external factors for missing points, which results in suboptimal performance.

For the trajectory point embedder, excluding road network for observed points causes the model to rely solely on latitude and longitude, neglecting the relationship between trajectories and the road network, which demonstrates that road network is crucial for accurately modeling trajectory information. Additionally, removing reference tokens results in a performance decline, as PLMs are unable to directly interpret trajectory data.

6 Conclusion

In this paper, we propose PTR, a novel framework for trajectory recovery leveraging PLM. PTR efficiently handles trajectory recovery even with limited dense trajectory data, demonstrating strong scalability. The model is trained on datasets with various sparse trajectories, enabling it to effectively generalize to different sampling intervals. To model external factors, we introduce an implicit trajectory prompt to model road conditions, which provides rich information for missing trajectory points. We also develop a trajectory embedder to capture the spatial-temporal dependencies of sparse trajectories and convert them into a format interpretable by PLMs. Experimental results on two datasets with three different sampling intervals validate the efficacy and scalability of the proposed model.

References

- [1] Prithu Banerjee, Sayan Ranu, and Sriram Raghavan. 2014. Inferring uncertain trajectories from partial observations. In *2014 IEEE International Conference on Data Mining*. IEEE, 30–39.
- [2] Dawei Chen, Cheng Soon Ong, and Lexing Xie. 2016. Learning points and routes to recommend trajectories. In *Proceedings of the 25th ACM international conference on information and knowledge management*. 2227–2232.
- [3] Wei Chen, Yuxuan Liang, Yuanshao Zhu, Yanchuan Chang, Kang Luo, Haomin Wen, Lei Li, Yanwei Yu, Qingsong Wen, Chao Chen, et al. 2024. Deep learning for trajectory data management and mining: A survey and beyond. *arXiv preprint arXiv:2403.14151* (2024).
- [4] Yile Chen, Gao Cong, and Cuauhtemoc Anda. 2023. Teri: An effective framework for trajectory recovery with irregular time intervals. *Proceedings of the VLDB Endowment* 17, 3 (2023), 414–426.
- [5] Yuqi Chen, Hanyuan Zhang, Weiwei Sun, and Baihua Zheng. 2023. Rntrajrec: Road network enhanced trajectory recovery with spatial-temporal transformer. In *2023 IEEE 39th International Conference on Data Engineering (ICDE)*. IEEE, 829–842.
- [6] Zaiben Chen, Heng Tao Shen, and Xiaofang Zhou. 2011. Discovering popular routes from trajectories. In *2011 IEEE 27th International Conference on Data Engineering*. IEEE, 900–911.
- [7] Jacob Devlin, Ming-Wei Chang, Kenton Lee, and Kristina Toutanova. 2018. Bert: Pre-training of deep bidirectional transformers for language understanding. *arXiv preprint arXiv:1810.04805* (2018).
- [8] Shengnan Guo, Youfang Lin, Letian Gong, Chenyu Wang, Zeyu Zhou, Zekai Shen, Yiheng Huang, and Huaiyu Wan. 2023. Self-supervised spatial-temporal bottleneck attentive network for efficient long-term traffic forecasting. In *2023 IEEE 39th International Conference on Data Engineering (ICDE)*. IEEE, 1585–1596.
- [9] Sahar Hoteit, Stefano Secchi, Stanislav Sobolevsky, Carlo Ratti, and Guy Pujolle. 2014. Estimating human trajectories and hotspots through mobile phone data. *Computer Networks* 64 (2014), 296–307.
- [10] Edward J Hu, Yelong Shen, Phillip Wallis, Zeyuan Allen-Zhu, Yuanzhi Li, Shean Wang, Lu Wang, and Weizhu Chen. 2021. Lora: Low-rank adaptation of large language models. *arXiv preprint arXiv:2106.09685* (2021).
- [11] Juho Lee, Yoonho Lee, Jungtaek Kim, Adam Kosiorek, Seungjin Choi, and Yee Whye Teh. 2019. Set transformer: A framework for attention-based permutation-invariant neural networks. In *International conference on machine learning*. PMLR, 3744–3753.
- [12] Xiucheng Li, Kaiqi Zhao, Gao Cong, Christian S Jensen, and Wei Wei. 2018. Deep representation learning for trajectory similarity computation. In *2018 IEEE 34th international conference on data engineering (ICDE)*. IEEE, 617–628.
- [13] Yang Li, Si Si, Gang Li, Cho-Jui Hsieh, and Samy Bengio. 2021. Learnable fourier features for multi-dimensional spatial positional encoding. *Advances in Neural Information Processing Systems* 34 (2021), 15816–15829.
- [14] Paul Newson and John Krumm. 2009. Hidden Markov map matching through noise and sparseness. In *Proceedings of the 17th ACM SIGSPATIAL international conference on advances in geographic information systems*. 336–343.
- [15] Adam Paszke, Sam Gross, Francisco Massa, Adam Lerer, James Bradbury, Gregory Chanan, Trevor Killeen, Zeming Lin, Natalia Gimelshein, Luca Antiga, et al. 2019. Pytorch: An imperative style, high-performance deep learning library. *Advances in neural information processing systems* 32 (2019).
- [16] Zeenat Rehena and Marijn Janssen. 2018. Towards a framework for context-aware intelligent traffic management system in smart cities. In *Companion Proceedings of the The Web Conference 2018*. 893–898.
- [17] Huimin Ren, Sijie Ruan, Yanhua Li, Jie Bao, Chuishi Meng, Ruiyuan Li, and Yu Zheng. 2021. Mtrajrec: Map-constrained trajectory recovery via seq2seq multi-task learning. In *Proceedings of the 27th ACM SIGKDD Conference on Knowledge Discovery & Data Mining*. 1410–1419.
- [18] Yilong Ren, Yue Chen, Shuai Liu, Boyue Wang, Haiyang Yu, and Zhiyong Cui. 2024. TPLLM: A Traffic Prediction Framework Based on Pretrained Large Language Models. *arXiv preprint arXiv:2403.02221* (2024).
- [19] Junjun Si, Jin Yang, Yang Xiang, Hanqiu Wang, Li Li, Rongqing Zhang, Bo Tu, and Xiangqun Chen. 2023. TrajBERT: BERT-Based Trajectory Recovery with Spatial-Temporal Refinement for Implicit Sparse Trajectories. *IEEE Transactions on Mobile Computing* (2023).
- [20] Han Su, Kai Zheng, Haozhou Wang, Jiamin Huang, and Xiaofang Zhou. 2013. Calibrating trajectory data for similarity-based analysis. In *Proceedings of the 2013 ACM SIGMOD international conference on management of data*. 833–844.
- [21] Hao Sun, Changjie Yang, Liwei Deng, Fan Zhou, Feiteng Huang, and Kai Zheng. 2021. Periodicmove: Shift-aware human mobility recovery with graph neural network. In *Proceedings of the 30th ACM International Conference on Information & Knowledge Management*. 1734–1743.
- [22] Matthew Tancik, Pratul Srinivasan, Ben Mildenhall, Sara Fridovich-Keil, Nithin Raghavan, Utkarsh Singhal, Ravi Ramamoorthi, Jonathan Barron, and Ren Ng. 2020. Fourier features let networks learn high frequency functions in low dimensional domains. *Advances in neural information processing systems* 33 (2020), 7537–7547.
- [23] Jingyuan Wang, Ning Wu, Xinxi Lu, Wayne Xin Zhao, and Kai Feng. 2019. Deep trajectory recovery with fine-grained calibration using kalman filter. *IEEE Transactions on Knowledge and Data Engineering* 33, 3 (2019), 921–934.
- [24] Qinyong Wang, Hongzhi Yin, Tong Chen, Zi Huang, Hao Wang, Yanchang Zhao, and Nguyen Quoc Viet Hung. 2020. Next point-of-interest recommendation on resource-constrained mobile devices. In *Proceedings of the Web conference 2020*. 906–916.
- [25] Sheng Wang, Zhifeng Bao, J Shane Culpepper, and Gao Cong. 2021. A survey on trajectory data management, analytics, and learning. *ACM Computing Surveys (CSUR)* 54, 2 (2021), 1–36.
- [26] Yu Wang, Tongya Zheng, Yuxuan Liang, Shunyu Liu, and Mingli Song. 2024. Cola: Cross-city mobility transformer for human trajectory simulation. In *Proceedings of the ACM on Web Conference 2024*. 3509–3520.
- [27] Tonglong Wei, Youfang Lin, Yan Lin, Shengnan Guo, Lan Zhang, and Huaiyu Wan. 2024. Micro-Macro Spatial-Temporal Graph-Based Encoder-Decoder for Map-Constrained Trajectory Recovery. *IEEE Transactions on Knowledge and Data Engineering* (2024).
- [28] Tong Xia, Yunhan Qi, Jie Feng, Fengli Xu, Funing Sun, Diansheng Guo, and Yong Li. 2021. Attnmove: History enhanced trajectory recovery via attentional network. In *Proceedings of the AAAI conference on artificial intelligence*, Vol. 35. 4494–4502.
- [29] Fengli Xu, Zhen Tu, Yong Li, Pengyu Zhang, Xiaoming Fu, and Depeng Jin. 2017. Trajectory recovery from ash: User privacy is not preserved in aggregated mobility data. In *Proceedings of the 26th international conference on world wide web*. 1241–1250.
- [30] Shuai Xu, Donghai Guan, Zhuo Ma, and Qing Meng. 2022. A Temporal-Context-Aware Approach for Individual Human Mobility Inference Based on Sparse Trajectory Data. In *Asia-Pacific Web (APWeb) and Web-Age Information Management (WAIM) Joint International Conference on Web and Big Data*. Springer, 106–120.
- [31] Peilun Yang, Hanchen Wang, Ying Zhang, Lu Qin, Wenjie Zhang, and Xuemin Lin. 2021. T3s: Effective representation learning for trajectory similarity computation. In *2021 IEEE 37th International Conference on Data Engineering (ICDE)*. IEEE, 2183–2188.
- [32] Pengpeng Zhao, Anjing Luo, Yanchi Liu, Jiajie Xu, Zhixu Li, Fuzhen Zhuang, Victor S Sheng, and Xiaofang Zhou. 2020. Where to go next: A spatio-temporal gated network for next poi recommendation. *IEEE Transactions on Knowledge and Data Engineering* 34, 5 (2020), 2512–2524.
- [33] Kai Zheng, Yu Zheng, Xing Xie, and Xiaofang Zhou. 2012. Reducing uncertainty of low-sampling-rate trajectories. In *2012 IEEE 28th international conference on data engineering*. IEEE, 1144–1155.

A Dataset

B Baseline Setting

We choose the following ten methods as baselines, including five free space trajectory recovery and five map-matched trajectory recovery.

Table 4: Dataset Description.

Types	Chengdu	Porto
Sampling interval	15s	15s
# Trajectory	118,354	322,079
# Road segment	2504	2224
Latitude range	30.655 ~ 30.727	41.142 ~ 41.174
Longitude range	104.043 ~ 104.129	-8.652 ~ -8.578
Length / Width	8.22 km / 8.00 km	6.19 km / 3.56 km

B.1 Free-space Trajectory Recovery

Free space trajectory recovery first recovers trajectory points and then projects the trajectory onto the road network.

- **HMM [14] + ShortestPath** first projects the sparse trajectory on the road network based on the hidden markov model (HMM), and then calculate the shortest path.
- **Linear [9] + HMM [14]** linearly interpolates missing trajectory points and then implements HMM to perform the map matching process.
- **MPR [6] + HMM [14]** first divides the area of interest into grids to identify frequently traveled routes between sparse trajectory points. Then, it assumes that vehicle movement maintains a constant speed for trajectory recovery. Subsequently, it employs HMM to project the trajectory onto the road network.
- **DHTR [23] + HMM [14]** incorporates a sequence-to-sequence framework and Kalman filtering to recover trajectory points. Subsequently, it applies an HMM to yield a trajectory that is constrained by the map.
- **AttnMove [28] + Rule** uses attention to predict the missing road segments and uses the central location as the moving rate.

B.2 Map-matched Trajectory Recovery

Map-matched trajectory recovery can directly recover the trajectory on the road network.

- **MTrajRec [17]** utilizes a sequence-to-sequence framework with Gated Recurrent Units (GRU) as the key component for trajectory recovery. It optimizes road segment and moving rate prediction through multi-task learning.
- **T2vec [12] + Decoder** is a deep learning model for trajectory similarity learning. We use its encoder to embed the sparse trajectory and use the decoder of the MTrajRec to recover the trajectory in an autoregressive manner.
- **T3s [31] + Decoder** uses LSTM and attention mechanisms to encode sparse trajectory data effectively. Then, the MTrajRec decoder is utilized to recover the trajectory.
- **RNTrajRec [5]** leverages the Transformer to capture the spatial-temporal correlation of the sparse trajectories. It also takes into account the relation between the trajectory and the road network.
- **MM-STGED [27]** models sparse trajectories from a graph perspective and recovers trajectories by capturing micro and macro semantic information.

C Evaluation Metrics

We adopt five widely used metrics to evaluate the effectiveness of our model, following previous works [5, 17, 27]. For road segment

recovery, we use **Accuracy (Acc)**, **Recall**, and **Precision (Prec)** to assess the alignment between the true road segments $\mathcal{E}_p = \{e_1, \dots, e_m\}$ and the predicted road segments $\hat{\mathcal{E}}_p = \{\hat{e}_1, \dots, \hat{e}_m\}$. A higher value in these metrics indicates a more accurate road segment recovery. The metrics are formally defined as follows:

$$\begin{aligned} \text{Acc} &= \frac{1}{m} \sum_{i=1}^m \mathbb{1}\{e_i = \hat{e}_i\} \times 100\%, \\ \text{Recall} &= \frac{|\mathcal{E}_p \cap \hat{\mathcal{E}}_p|}{|\hat{\mathcal{E}}_p|} \times 100\%, \\ \text{Prec} &= \frac{|\mathcal{E}_p \cap \hat{\mathcal{E}}_p|}{|\mathcal{E}_p|} \times 100\%, \end{aligned} \quad (17)$$

where $\mathbb{1}\{\cdot\}$ is the indicator function, where $e_i = \hat{e}_i$, $\mathbb{1}\{e_i = \hat{e}_i\} = 1$, otherwise $\mathbb{1}\{e_i = \hat{e}_i\} = 0$.

To evaluate the recovered GPS coordinates, we employ the **Mean Absolute Error (MAE)** and **Root Mean Square Error (RMSE)** to quantify the distance error between the true trajectory $\mathcal{T}_m = q_1, \dots, q_{|\mathcal{T}_m|}$ and the predicted trajectory $\hat{\mathcal{T}}_m = \hat{q}_1, \dots, \hat{q}_{|\hat{\mathcal{T}}_m|}$. The formulas for MAE and RMSE are given as follows: The formulas of MAE and RMSE are as follows:

$$\begin{aligned} \text{MAE} &= \frac{1}{|\mathcal{T}_m|} \sum_{i=1}^{|\mathcal{T}_m|} |\text{RN_dist}(q_i, \hat{q}_i)|, \\ \text{RMSE} &= \sqrt{\frac{1}{|\mathcal{T}_m|} \sum_{i=1}^{|\mathcal{T}_m|} |\text{RN_dist}(q_i, \hat{q}_i)|^2} \end{aligned} \quad (18)$$

Here, following [5, 17, 27], $\text{RN_dist}(q, \hat{q})$ signifies the shortest distance along the road network between the trajectory points q and \hat{q} . Both MAE and RMSE are denoted in meters. Lower values of these metrics indicate a higher level of accuracy in the recovery results.

D Appendix Experiments

D.1 Convergence Rate

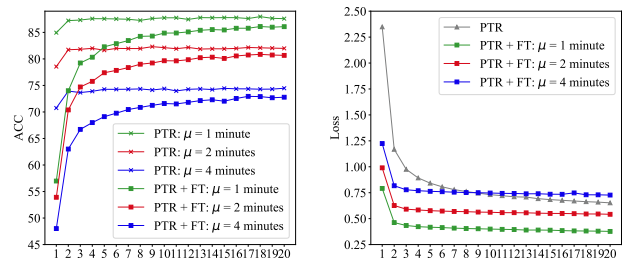


Figure 5: Convergence rate of PTR and fine-tuning for three sampling intervals on Chengdu.

We evaluate the convergence speed of our model on the Porto and Chengdu datasets. As illustrated in Figure 5 and 6, the model reaches near-optimal performance by the 10th epoch. The trained model demonstrated robust accuracy across three sampling intervals (PTR: $u = 1$ minute, PTR: $u = 2$ minutes, and PTR: $u = 4$ minutes), confirming that PTR can generalize effectively to sparse trajectories

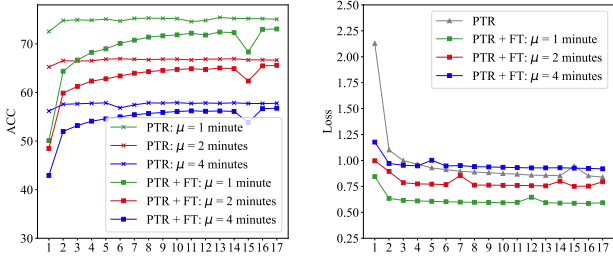


Figure 6: Convergence rate of PTR and fine-tuning for three sampling intervals on Porto.

Table 5: Hyperparameter range and optimal value.

Parameter	Range
The number of reference tokens K	128, 256, <u>512</u> , 1024
LoRA rank r	4, 8, 16, 64
The loss function weight λ	0.1, 1, <u>10</u> , 100

with varying sampling intervals. Furthermore, after fine-tuning at each sampling interval, the performance shows minimal change in performance by the 3rd epoch, further proving its fast convergence speed.

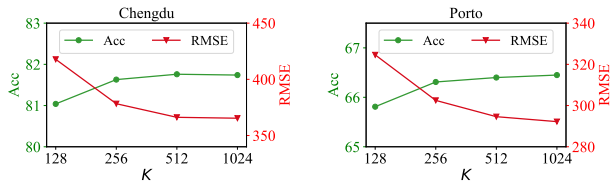


Figure 7: Hyperparameter analysis of the number of reference tokens K of trajectory feature transformation.

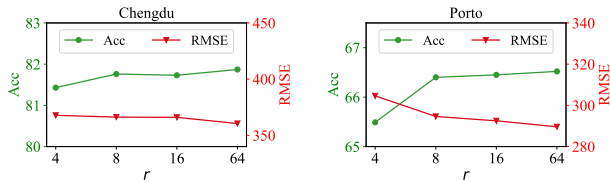


Figure 8: Hyperparameter analysis of the rank r of LoRA.

D.2 Hyperparameter Study

To explore the impact of hyperparameters on model performance, we conduct hyperparameter analysis using the Chengdu and Porto datasets with the sparse trajectory sampling interval of 2 minutes. We consider three important hyperparameters, including the number of reference tokens K , the rank r of LoRA, and the loss function

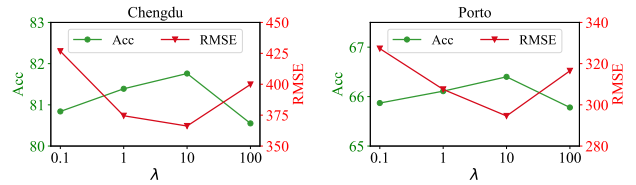


Figure 9: Hyperparameter analysis of the weight λ in the loss function.

weight λ . Details regarding the range of selection and the optimal values for these hyperparameters are presented in Table 5.

D.2.1 The Number of Reference Tokens K . We set the parameter K from the set $\{128, 256, 512, 1024\}$ to explore its impact on trajectory recovery. The experimental results are shown in Figure 7. As K increases, the effectiveness of trajectory recovery also improves. This suggests that having a larger token space aids in accurately representing trajectory features. When K is larger than 512, the performance improvement of PTR becomes marginal, while the computational cost will increase. To balance the performance and efficiency of the model, we set K to 512.

D.2.2 The Rank r of LoRA. As shown in Figure 8, we set the range of r to 4, 8, 16, and 64 to explore its impact. It is observed that the model performs well when $r = 4$. As r increases, the accuracy will continue to increase, but it is not obvious. This suggests that PLMs encapsulate substantial domain expertise through training on extensive corpora, rendering them adaptable to trajectory recovery tasks with minor adjustments. Yet as r increases, the number of parameters also increases, making the model training require more memory. Therefore, we set $r = 8$ to balance the performance and resources.

D.2.3 The Loss Weight λ . As shown in Figure 9, as the loss function weight λ increases, the model performance first improves and then decreases. This is because a smaller λ will make the model focus on road segment recovery, while a larger λ will focus on moving rate recovery. To balance these two tasks, we set the value of λ to 10.

D.3 Case Study

We conduct a case study on the Chengdu dataset to visualize the trajectory recovery performance with various baselines. As shown in Figure 10, we draw the truth and recovered trajectory, where red points represent the truth trajectory points and blue points indicate the recovered trajectory points. We find that the recovered trajectory aligns well with the road network, demonstrating the effectiveness of using road segment and moving rate to represent trajectory point. To facilitate a more intuitive comparison of recovery performance among different models, we focus on two distinct regions, labeled as A and B, for visual analysis. In region A, characterized by a relatively simple road network structure, all models can accurately recover road segments. Among them, PTR maps trajectory points better by leveraging PLMs. In contrast, region B exhibits a more intricate road network with multiple accessible

Table 6: Computation Cost.

Dataset	Chengdu / Porto		
	Methods	Model size (MBytes)	Train time (min/epoch)
DHTR	19 / 18	11.30 / 42.55	1.13 / 2.35
MTrajRec	49 / 44	37.19 / 142.12	12.57 / 28.20
RNTrajRec	112 / 109	72.30 / 153.29	29.14 / 43.58
MM-STGED	34 / 31	41.27 / 138.33	16.27 / 30.58
PTR	176 / 175	24.18 / 54.14	2.56 / 10.38

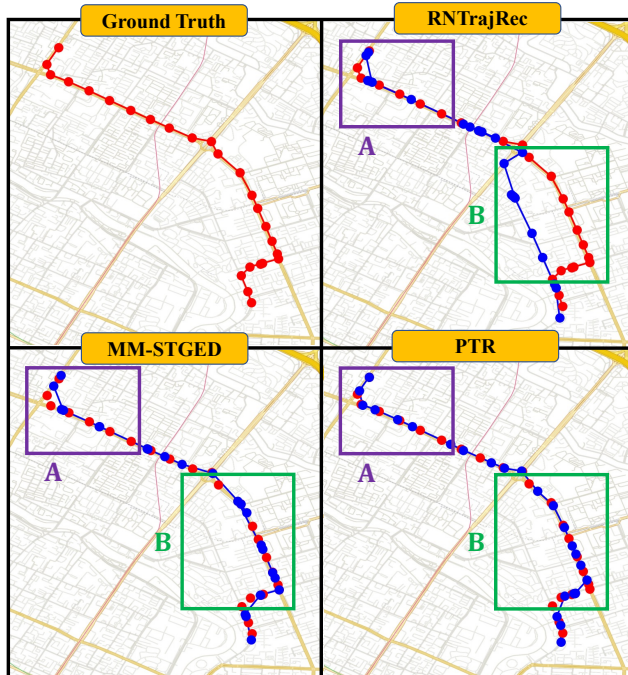


Figure 10: Case study on the Chengdu dataset. Red points represent the truth trajectory points and blue points represent the recovered trajectory points.

routes. RNTrajRec captures spatial-temporal correlations of trajectories that are not adequate and recovers incorrect road segments. PTR not only excels in road segment recovery but also in accurately matching the actual trajectory points. This success can be attributed to its ability to model missing trajectory points through the implicit trajectory prompt, thereby introducing more valuable information and improving performance.

D.4 Computational Cost

We use an NVIDIA RTX A4000 card to conduct cost analysis on the Chengdu and Porto datasets with a 2-minute sampling interval by considering model size, training time, and inference time. As shown in Table 6, compared to the end-to-end deep learning model, PTR has the largest number of parameters due to its utilization of a pre-trained language model based on the BERT-small framework. Despite having a greater number of parameters, PTR exhibits quicker training and testing times as it can output results for all trajectory points at once, and the majority of parameters are frozen, unlike other models that necessitate autoregressive generation. It significantly accelerates both model training and inference processes.